Appl. Phys. B 67, 23–28 (1998)

Applied Physics B
Lasers
and Optics

Cross sections of excited-state absorption at 800 nm in erbium-doped ZBLAN fiber

M. Pollnau, Ch. Ghisler, W. Lüthy, H.P. Weber

Institute of Applied Physics, University of Bern, Sidlerstrasse 5, CH-3012 Bern, Switzerland
(Fax: +41-31/631-3765, E-mail: luethy@iap.unibe.ch)

Received: 20 January 1998

Abstract. Excited-state absorption (ESA) from the metastable levels $^4I_{13/2}$ and $^4I_{11/2}$ of erbium is measured in a fluorozirconate fiber in the wavelength range 780–840 nm. Using a pump- and probe-beam technique and choosing the pump wavelength such that the perturbation by pump ESA is minimized in the measurement, it is possible to determine the effective ESA cross sections, despite the fact that the excitation is distributed among two metastable levels. The derived ESA cross sections at 793 nm of 1.4×10^{-21} cm^2 from the $^4I_{13/2}$ level and less than 0.1×10^{-21} cm^2 from the $^4I_{11/2}$ level are in reasonable agreement with former results obtained from a rate-equation simulation of the erbium 3-μm laser. The corresponding ESA spectrum under 3-μm lasing conditions is derived. At the strongest ground-state absorption around 799 nm, decreasing ESA from the $^4I_{13/2}$ level is compensated by increasing ESA from the $^4I_{11/2}$ level, i.e., ESA losses cannot be avoided when pumping around 800 nm. This result is of relevance for possible high-power diode pumping of an erbium 3-μm double-clad fiber laser.

PACS: 42.55.Wd; 42.60.Lh; 78.30.-j

In recent years, research in the field of lasers emitting at 3 μm has been strongly stimulated by their potential applications in laser surgery [1]. Due to the high absorption of 3-μm radiation in water, high-quality cutting or ablation is demonstrated in biological tissue using erbium-doped solid-state lasers [2, 3]. Erbium-doped fluoride fibers are promising candidates for the construction of compact and efficient all-solid-state laser sources that provide large flexibility and high laser intensity, which are of relevance for surgical applications.

In ZBLAN fibers, excited-state absorption (ESA) at 792 nm from the $^4I_{13/2}$ lower laser level was found to have a major influence on the lasing properties of the erbium 3-μm transition [4]. This ESA depletes the lower laser level and assists in establishing inversion between the 3-μm laser levels. On the other hand, it populates the $^4S_{3/2}$ level and leads to competitive lasing at 850 nm, which causes a saturation of the 3-μm output power [5]. Cascade-lasing schemes which recycle the upconverted energy can avoid this saturation [6, 7]. Unfortunately, these schemes are restricted to high-intensity Ti:sapphire pumping. An approach has been suggested recently, which aims to avoid pump ESA and requires only low pump intensity, thus enabling high-power double-clad diode pumping of the erbium 3-μm fiber laser [8]. However, the values of the relevant ESA cross sections could not be determined experimentally so far, because the pump excitation is distributed between two metastable levels of erbium in ZBLAN, and ESA transitions from these two levels overlap in the spectral region of interest [9]. Whether a strong influence of ESA can be avoided in the pump band at 800 nm has, therefore, been an open question.

In this paper, we present measured ESA spectra of ZBLAN:Er^{3+} in the wavelength range 780–840 nm of the $^4I_{15/2} \rightarrow {}^4I_{9/2}$ pump transition under non-lasing conditions. Effective excited-state cross sections of the transitions from the $^4I_{11/2}$ and $^4I_{13/2}$ metastable levels are derived and an approximate ESA spectrum under lasing conditions is calculated. Results are compared to cross sections obtained from a rate-equation simulation of the erbium 3-μm laser. With the derived ESA spectra, the experimental results of several publications can be explained.

1 Experimental

A pump- and probe-beam technique [10, 11] is used for the measurement of quasi-cw-pumped ESA spectra. The experimental arrangement is shown in Fig. 1. It is similar to those used in [9, 12–14]. The investigated fiber has a length of $d = 0.8$ m, a core radius of $\omega = 3.25$ μm, and an erbium concentration of $N_d = 1.6 \times 10^{19}$ cm^{-3} (= 1000 ppm mol. in ZBLAN). Pump radiation at $\lambda_p = 987.3$ nm or $\lambda_p = 995.0$ nm from a Ti:sapphire laser is absorbed on the ground-state transition $^4I_{15/2} \rightarrow {}^4I_{11/2}$ as well as on the excited-state transition $^4I_{11/2} \rightarrow {}^4F_{7/2}$, see Fig. 2 (left-hand side). Three measurements are performed with different pump wavelengths and input powers. The pump wavelengths λ_p, cross sections σ_{ij} of

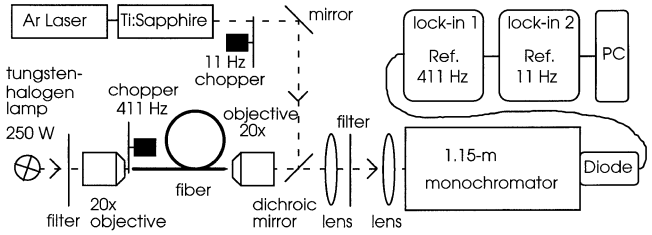

Fig. 1. Experimental arrangement for the measurement of ESA in fibers

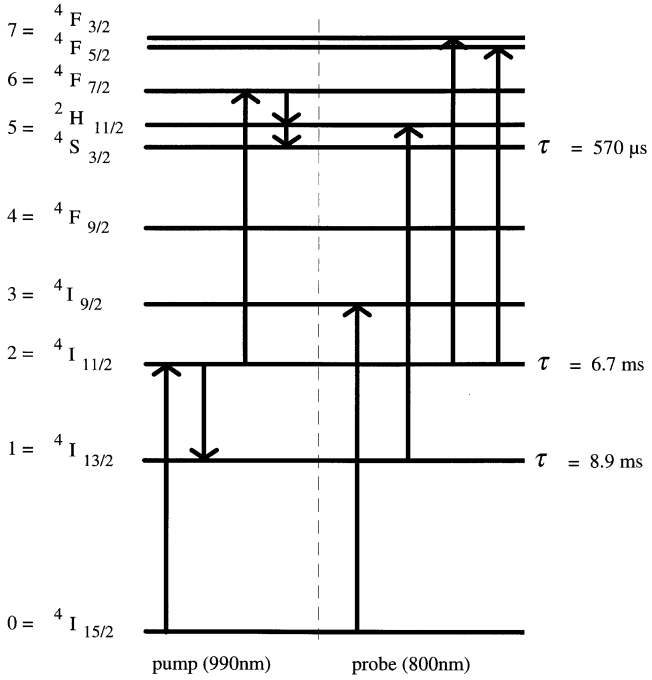

Fig. 2. Energy-level diagram of ZBLAN:Er^{3+} indicating the pump excitation of the system at 987–995 nm (*left-hand side*) and the transitions detected by the probe beam at 780–840 nm (*right-hand side*)

ground-state absorption (GSA) and ESA, and incident pump powers P_{inc} of the measurements are summarized in Table 1. A fraction of $\eta_{\mathrm{in}} < 30\%$ of the pump power is launched into the fiber.

Broadband probe light from a 250-W halogen lamp is focused into the fiber. The transmitted spectrum of the counter-propagating probe beam at $\lambda_t = 780$–840 nm passes through a monochromator (1.15-m spectrometer, resolution 1 nm) and is detected with an optical photodiode. The probe light is chopped with a frequency of 411 Hz and amplified with a first lock-in amplifier to discriminate reflected pump light and fluorescence from the sample. The transmitted probe-beam intensity I_u in the unpumped case is recorded from the unamplified output channel of the first lock-in amplifier. The pump beam is chopped with 11 Hz. With a second lock-in amplifier set at 11 Hz, the difference

$$\Delta I = A(I_p - I_u) \tag{1}$$

between the transmitted probe-beam intensities I_p and I_u in the pumped and unpumped case is measured and recorded on a PC. The amplification factor A of the first lock-in amplifier is determined from measuring the amplification of a known signal. The spectra are obtained from the measurements of ΔI with (1) and

$$-\ln[1 + (\Delta I/A)/I_u] = \ln[I_u/I_p]\,. \tag{2}$$

The three spectra measured in our experiments are shown in Fig. 3a. The GSA cross section $\sigma_{\mathrm{GSA}}(\lambda_t)$, cf. the thick line in Fig. 4b, is determined in a separate measurement. The differences in cross sections σ of ESA originating from level i at wavelength λ_t are then calculated from the GSA and $\ln[I_u/I_p]$

Table 1. Pump parameters of the three different ESA measurements

Parameter	Ref.	Measurement A	Measurement B	Measurement C
λ_p		987.3 nm	987.3 nm	995.0 nm
$\sigma_{02}(\lambda_p)$	[20]	6.1×10^{-22} cm^2	6.1×10^{-22} cm^2	3.9×10^{-22} cm^2
$\sigma_{26}(\lambda_p)$	[20]	1.7×10^{-22} cm^2	1.7×10^{-22} cm^2	0.6×10^{-22} cm^2
$P_{\mathrm{inc}}(\lambda_p)$		51 mW	17 mW	48 mW

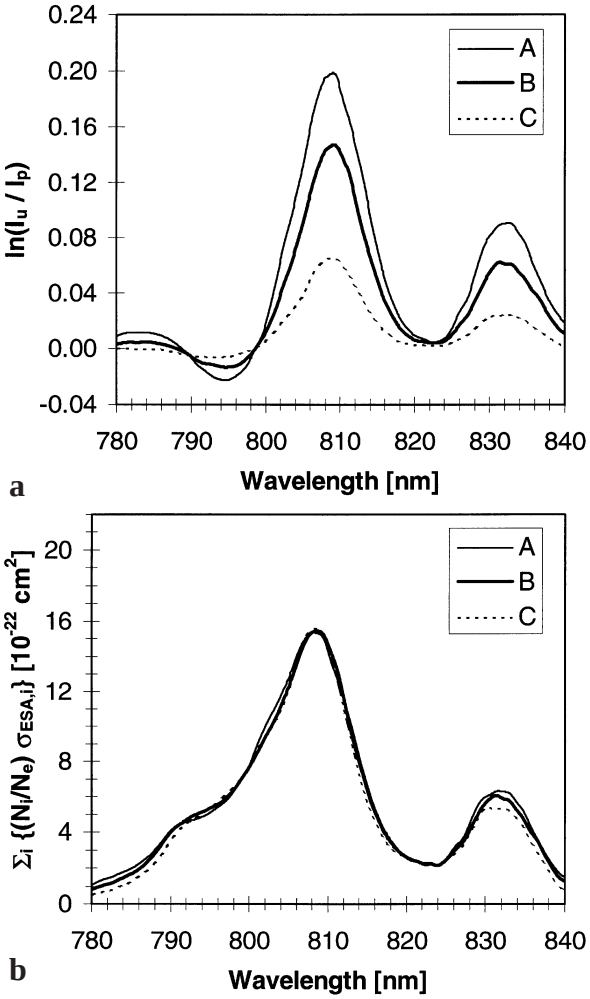

Fig. 3. a Measured spectra of $-\ln[1 + \Delta T/T] = \ln[I_u/I_p]$ and **b** spectra (calculated from **a**) of the cross sections of excited-state absorption times the relative population densities N_i/N_e of the $^4I_{13/2}$ and $^4I_{11/2}$ levels under non-lasing conditions, for the three different experiments A, B, and C

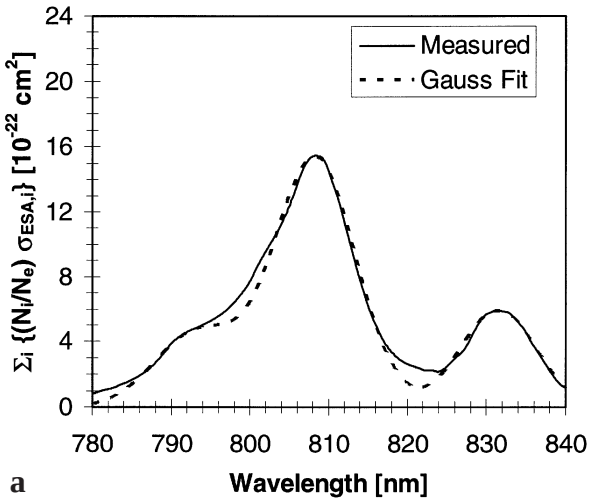

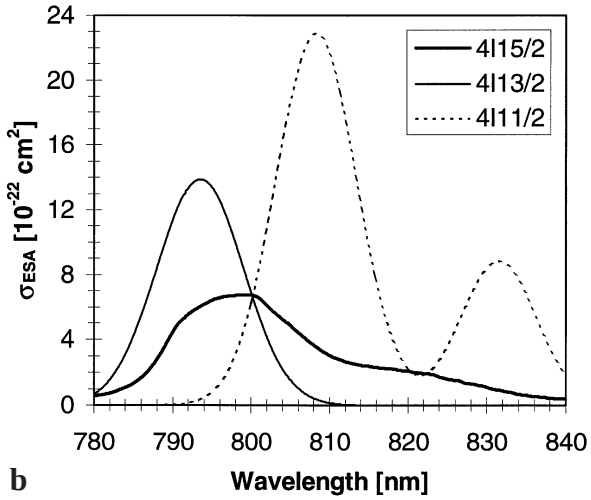

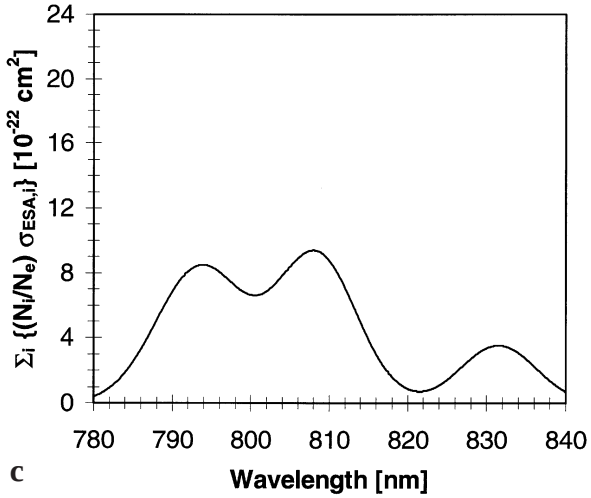

Fig. 4. a Average of the spectra A, B, and C of Fig. 3b and fit by the sum of three Gaussian functions. **b** Effective cross sections of the absorption transitions of ZBLAN:Er^{3+} in the pump-wavelength range at 800 nm: Measured GSA transition $^4I_{15/2} \rightarrow {}^4I_{9/2}$ (799 nm) and Gaussian fits of the ESA transitions $^4I_{13/2} \rightarrow {}^2H_{11/2}$ (793 nm), $^4I_{11/2} \rightarrow {}^4F_{3/2}$ (808 nm), and $^4I_{11/2} \rightarrow {}^4F_{5/2}$ (831 nm). **c** ESA from the $^4I_{13/2}$ and $^4I_{11/2}$ laser levels under conditions of threshold inversion for the 3-μm laser for an outcoupling degree of $R = 50\%$ (relative excitation densities $N_i/N_e = 60\%$ and 40%, respectively)

spectra using the equation [11]

$$\sum_i [(N_i/N_e)\sigma_{ESA,i}] = \ln[I_u/I_p]/(N_e\,d) + \sigma_{GSA}\,. \qquad (3)$$

The sum in (3) extends over all metastable levels which have a substantial relative population density N_i/N_e. The total excitation density N_e can be derived directly from the calculation of (3) at wavelengths where no ESA is present. The parameter N_e is determined correctly if the measured bleaching of the GSA in the $\ln[I_u/I_p]$ spectrum is compensated by the addition of the GSA spectrum in (3). In ZBLAN:Er^{3+}, ESA is present over the whole spectral range of GSA from 780–840 nm and N_e can only be determined with a relatively high error margin, cf. Sect. 2. Spectra of the effective ESA cross sections $\sigma_{ESA,i}$ times the relative population densities N_i/N_e, as calculated from the measured data of Fig. 3a and using (3), are shown in Fig. 3b.

2 Results

The knowledge of the relative population densities N_i/N_e is required in order to derive the effective ESA cross sections $\sigma_{ESA,i}$ from (3). If time-resolved ESA measurements are performed, the two variables can be separated and the required information can be obtained directly from the spectra [11]. In the present case, cw-pumped ESA spectra are measured and information on the relative population densities has to be derived from analytical rate-equation solutions which are explained in this section.

2.1 Relative population densities under non-lasing conditions

The rate equations without laser operation and under the pump conditions described in Sect. 1 consider the $^4I_{15/2}$ ground state (level 0) as well as the metastable levels $^4I_{13/2}$ (1), $^4I_{11/2}$ (2), and $^4S_{3/2}$ (5). The erbium lifetimes τ_i in ZBLAN which are given in Fig. 2 are taken from [15]. The lifetimes of the other levels are rather small, and the excitations of these levels are negligible. The important branching ratios are calculated from Judd–Ofelt data of the radiative decay rates in ZBLAN [15] and from the fluorescence lifetimes of Fig. 2, under the assumption that the non-radiative decay rate into the next lower-lying level is given by the difference between the inverse fluorescence lifetime and the sum of the radiative rates. The relevant branching ratios derived in this way are $\beta_{21} = 0.37$, $\beta_{51} = 0.18$, and $\beta_{52} = 0.38$.

With the above considerations, the rate equations for the population densities N_i of the important levels read:

$$0 = dN_5/dt = R_{26} - \tau_5^{-1}N_5\,, \qquad (4)$$

$$0 = dN_2/dt = R_{02} - R_{26} - \tau_2^{-1}N_2 + \beta_{52}\tau_5^{-1}N_5\,, \qquad (5)$$

$$0 = dN_1/dt = -\tau_1^{-1}N_1 + \beta_{21}\tau_2^{-1}N_2 + \beta_{51}\tau_5^{-1}N_5\,, \qquad (6)$$

$$N_d = N_0 + N_e = N_0 + N_1 + N_2 + N_5\,. \qquad (7)$$

The excitation of the $^4F_{7/2}$ level (labeled level 6 here for consistency with other publications), which is induced by the

ESA rate R_{26}, decays rapidly to the $^4S_{3/2}$ level (5). We derive the following solutions of the rate-equation system (4)–(7):

$$N_2/N_e = \left[1 + \left(\beta_{21}\tau_2^{-1} + \beta_{51}R_{26}\right)/\tau_1^{-1} + R_{26}/\tau_5^{-1}\right]^{-1}, \quad (8)$$

$$N_1/N_e = \left[1 + \tau_1^{-1}/\left(\beta_{21}\tau_2^{-1} + \beta_{51}R_{26}\right)\left(1 + R_{26}/\tau_5^{-1}\right)\right]^{-1}. \quad (9)$$

Since the lifetime τ_5 of the $^4S_{3/2}$ level is rather small and the pump wavelength was chosen in such a way that the ESA rate R_{26} has a small influence, i.e., the population of the $^4S_{3/2}$ level is small, the term R_{26}/τ_5^{-1} in (8) and (9) can be neglected. Introducing the abbreviations

$$X = X_0 + \delta X = \left(\beta_{21}\tau_2^{-1}/\tau_1^{-1}\right) + \left(\beta_{51}R_{26}/\tau_1^{-1}\right), \quad (10)$$

we can write (8) and (9) as

$$N_2/N_e = [1 + X]^{-1}, \quad (11)$$

$$N_1/N_e = [1 + 1/X]^{-1}. \quad (12)$$

The value X_0 is equal to the ratio of the population densities N_1 and N_2 in the absence of ESA (cf. [16]). The perturbation term δX describes the influence of ESA on the population densities N_1 and N_2. With h and c, Planck's constant and the vacuum speed of light, respectively, the equations for the pump rates R_{02} and R_{26} are given by (cf. [8])

$$\begin{aligned} R_{ij} = &\left[\sigma_{ij}N_i/\left(\sigma_{02}N_0 + \sigma_{26}N_2\right)\right] \\ &\times \{1 - \exp\left[d\left(\sigma_{02}N_0 + \sigma_{26}N_2\right)\right]\} \\ &\times \lambda_p/\left(hcd\pi\omega^2\right)\eta_{in}P_{inc}. \end{aligned} \quad (13)$$

It can be shown with the given experimental parameters that the perturbation δX introduced by pump ESA does not exceed 10% in (11) and (12) even at a rather high excitation density N_e. In our experiments, the excitation was smaller than $N_e = 0.15N_d$. Thus, the ratio of the relative excitation densities N_i/N_e in (3) is, with good approximation, given by the term X_0 in (10). This suggests that the three different measurements (cf. Table 1) will provide approximately the same calculated ESA spectra, because the multiplying factors N_i/N_e for the $^4I_{13/2}$ and $^4I_{11/2}$ levels are similar in the three experiments. This is indeed the case as can be seen from Fig. 3b. The values of the relative population densities under non-lasing conditions obtained from (11) and (12), if neglecting δX, are $N_1/N_e = 0.33$ and $N_2/N_e = 0.67$.

2.2 Relative population densities under lasing conditions

Under lasing conditions at the 3-μm transition, the population densities of the $^4I_{13/2}$ and $^4I_{11/2}$ levels are clamped to threshold inversion. We introduce a rate equation for the photon density ϕ [5, 8] which neglects spontaneous emission,

$$\begin{aligned} 0 = \mathrm{d}\phi/\mathrm{d}t = &(1/n_r)(b_2N_2 - b_1N_1)\sigma_{em}c\phi \\ &- [-\ln(Rf)]c\phi/(2n_rd), \end{aligned} \quad (14)$$

with n_r, the refractive index of ZBLAN, b_i, the Boltzmann factors of the lasing Stark levels, σ_{em}, the emission cross section, and Rf, the reflectance of the outcoupling mirror. From the solution of this equation, using the parameters for the 3-μm laser transition given in [5], typical results of $N_1/N_e = 0.6$ and $N_2/N_e = 0.4$ are derived under lasing conditions.

2.3 Determination of cross sections

Three peaks are observed in the spectra of Fig. 3b. By comparison with time-resolved ESA spectra of Er^{3+}:$YAlO_3$ [11], which allow the identification of the initial levels of the ESA transitions, we conclude that these peaks correspond to the transitions $^4I_{13/2} \rightarrow {}^2H_{11/2}$ (793 nm), $^4I_{11/2} \rightarrow {}^4F_{3/2}$ (808 nm), and $^4I_{11/2} \rightarrow {}^4F_{5/2}$ (831 nm), see Fig. 2 (right-hand side). It was suggested [9] that the peak at 831 nm originates from the $^4I_{9/2}$ level. However, this level has a small lifetime and its population is not high enough to introduce significant absorption from this level.

The calculated ESA spectra of Fig. 3b are averaged and fitted with the sum of three Gaussian functions, see Fig. 4a. This allows the separation of ESA from the $^4I_{13/2}$ and $^4I_{11/2}$ levels. Division of these functions by the relative population densities N_i/N_e of their initial levels under non-lasing conditions (Sect. 2.1) results in the spectral dependence of the effective ESA cross sections as displayed in Fig. 4b. The peak cross sections are $1.4 \times 10^{-21}\,\mathrm{cm}^2$ at 793 nm (from $^4I_{13/2}$), $2.3 \times 10^{-21}\,\mathrm{cm}^2$ at 808 nm (from $^4I_{11/2}$), and $0.9 \times 10^{-21}\,\mathrm{cm}^2$ at 831 nm (from $^4I_{11/2}$).

It was found during the calculation of the ESA spectra of Fig. 3b that the derivation of the excitation density N_e is not easy in the present case, because the measured spectra of Fig. 3a do not exhibit a strong spectral structure, this being a consequence of the strong linewidth broadening in the glass host. Whereas the measured ESA signal at 793 nm is close to zero (Fig. 3a) and the calculated peak cross section at this wavelength (Fig. 4b) does not vary significantly with the value chosen for N_e, the cross sections obtained in Fig. 4b for the ESA peaks at 808 and 831 nm exhibit a larger variation with N_e. The error margin at 808 nm is higher than 20%.

Once the spectral dependence of the effective ESA cross sections is known, the ESA spectra under any excitation can be calculated. We are particularly interested in the ESA features under lasing conditions at 3 μm. By multiplying the Gaussian functions of Fig. 4b with the relative population densities under lasing conditions (Sect. 2.2), the ESA spectrum of Fig. 4c is obtained, which indicates the spectral behavior of ESA under 3-μm laser operation.

3 Discussion

There are several experimental and calculated data available in literature, which give an indication of the expected ESA cross sections at certain pump wavelengths. In the following, those data will be compared with the results obtained in the present paper.

When ESA was utilized for the depletion of the 3-μm lower laser level and for the reduction of ground-state bleaching, the wavelength of 792 nm turned out to be the best choice [5–7]. Data of the ESA cross sections at this particular wavelength were obtained from rate-equation simulations of the performance of the erbium 3-μm ZBLAN laser [5]. Those values are $\sigma_{ESA}(^4I_{13/2}) = 1.0 \times 10^{-21}\,\mathrm{cm}^2$ and $\sigma_{ESA}(^4I_{11/2}) = 0.2 \times 10^{-21}\,\mathrm{cm}^2$. From the spectrum

of the effective ESA cross sections of Fig. 4b, values at the 793-nm peak wavelength of ESA of $\sigma_{\mathrm{ESA}}({}^4I_{13/2}) = 1.4 \times 10^{-21}\,\mathrm{cm}^2$ and $\sigma_{\mathrm{ESA}}({}^4I_{11/2}) < 0.1 \times 10^{-21}\,\mathrm{cm}^2$ are obtained. This shows that the rate-equation calculations provided values which are in reasonable agreement with the experimental data presented here, with some underestimation of the cross section from ${}^4I_{13/2}$, which was probably compensated by an overestimation of the emission cross section for the 850-nm laser line from the ${}^4S_{3/2}$ level in the calculations of [5].

The theoretical limit of the achievable slope efficiency at 3 μm when pumping at 792 nm depends on the loss introduced by pump ESA from the ${}^4I_{11/2}$ level [17]. Due to the smaller value of the ESA cross section of $\sigma_{\mathrm{ESA}}({}^4I_{11/2}) < 0.1 \times 10^{-21}\,\mathrm{cm}^2$ obtained here, this loss may be smaller than expected in [17]. This would increase the theoretical limit of the slope efficiency to 29.0% and reduce the relative value of the experimentally achieved slope efficiency of 25.4% [7] to 88% of the theoretical limit. However, it is not clear how well the Gaussian fit of the ESA peak at 808 nm reproduces the ESA cross section in its wing at 793 nm and how accurate the obtained value of the ESA cross section is.

A better indication of the correctness of the spectra presented here is given by comparison with experimental data of the threshold of 850-nm laser oscillation [18]. Both the ESA transitions from the ${}^4I_{13/2}$ and ${}^4I_{11/2}$ levels excite the ${}^4S_{3/2}$ upper laser level of the 850-nm line. A higher ESA cross section for either of the two transitions, therefore, reduces the threshold pump power for oscillation at 850 nm. The results of [18], which were obtained under simultaneous lasing at 3 μm, show the same double-peak structure as the ESA spectrum of Fig. 4c which also refers to lasing conditions at 3 μm. The almost equally low 850-nm threshold values at 792 and 808 nm [18] correspond to comparably high ESA (Fig. 4c) and GSA (Fig. 4b) cross sections at the same wavelengths, with the slightly smaller ESA at 792 nm compensated by a slightly stronger GSA compared to 808 nm and vice versa.

The ground-state laser transition at 1.55–1.6 μm from the ${}^4I_{13/2}$ level depends in the opposite way on the ESA cross sections. ESA from the ${}^4I_{13/2}$ level introduces a direct loss for this laser. ESA from the ${}^4I_{11/2}$ level decreases the feeding of the ${}^4I_{13/2}$ upper laser level from the ${}^4I_{11/2}$ level via multiphonon relaxation and fluorescence or lasing at 3 μm. It is, therefore, expected that, under conditions of simultaneous 3-μm lasing, this laser operates better in the wavelength range around 799–801 nm, which is in the dip between the two ESA peaks (Fig. 4c) and where the cross section of GSA is large (Fig. 4b). The strongest 1.55-μm fluorescence which depends solely on the excitation of the ${}^4I_{13/2}$ level is observed at 801 nm [19], where ESA losses have a minimum (Fig. 4c) and GSA is rather strong (Fig. 4b), whereas the lowest 1.6-μm laser threshold which also depends on the depletion of the ${}^4I_{15/2}$ lower laser level (the ground state), is obtained at 799 nm [18], where GSA is strongest (Fig. 4b) and ESA losses are rather small (Fig. 4c). The agreement of our spectra with the experimental results is evident.

In [8], a high-power diode-pumped 3-μm ZBLAN:Er^{3+} laser was predicted which will be capable of emitting 1 W of transversely single-mode output power. The implications of the present data for possible diode pumping of a 3-μm ZBLAN:Er^{3+} laser are as follows. ESA is present over the whole wavelength range of GSA from 780 to 840 nm, with ESA cross sections being equal to or larger than the GSA cross section (Fig. 4b). Therefore, when trying to operate the 3-μm ZBLAN:Er^{3+} laser as a simple four-level system, ESA losses cannot be avoided by choosing a different pump wavelength within this pump band. The dominance of GSA over ESA and operation as a four-level system can only be established when, firstly, effectively repopulating the ground state by quenching the lifetime of the ${}^4I_{13/2}$ lower laser level of the 3-μm transition via energy transfer to a co-doped rare-earth ion, secondly, using a high dopant concentration and, thirdly, applying a low pump intensity [8].

If the lifetime of the lower laser level is quenched by co-doping and depletion of this level via pump ESA loses its formerly positive influence [5–7], the pump band around 980 nm may be superior for pumping a double-clad ZBLAN:Er^{3+} laser operating at 3 μm. From the spectra of [20] it is apparent that pumping at 979 nm does not only provide a GSA cross section which is twice as large as at 799 nm and, hence, will strongly support absorption in a double-clad fiber as long as ground-state bleaching can be avoided. It also reduces the ESA cross section at 979 nm to $0.5 \times 10^{-21}\,\mathrm{cm}^2$, which is only one third of the GSA cross section at the same wavelength and slightly less than the ESA cross sections at 799 nm (Fig. 4b). In addition, pumping directly into the ${}^4I_{11/2}$ upper laser level provides a higher Stokes efficiency of the system than pumping into the ${}^4I_{9/2}$ level [21]. On the other hand, ESA at 979 nm originates from the ${}^4I_{11/2}$ upper laser level of the 3-μm transition, which is more detrimental to 3-μm lasing than ESA from the ${}^4I_{13/2}$ level.

The computer simulation of [8] is, therefore, reperformed for the pump wavelength of 979 nm. The calculation uses the same rate equations and parameters as in [8], but assumes pumping at 979 nm and absorption according to the measured cross sections [20] of GSA ${}^4I_{15/2} \rightarrow {}^4I_{11/2}$ and ESA ${}^4I_{11/2} \rightarrow {}^4F_{7/2}$ of $1.8 \times 10^{-21}\,\mathrm{cm}^2$ and $0.5 \times 10^{-21}\,\mathrm{cm}^2$, respectively. A larger cladding radius of 68.5 μm instead of 35.0 μm is chosen because of the increased GSA cross section at 979 nm compared to 792 nm. The simulation predicts that, while the cladding radius and the necessary pump-beam waist can be increased by a factor of 1.96, the output power of the fiber laser will increase from 1.0 to 1.5 W when pumping with 7 W of incident power at 979 nm. With increasing diode pump power and pump waist size and with corresponding adjustment of fiber parameters, even higher output powers will be achievable. Although ESA originates from the ${}^4I_{11/2}$ upper laser level now, its influence is kept extremely small by the measures explained in [8]. A wavelength of 979 nm will, therefore, be the pump wavelength of choice for a high-power diode-pumped double-clad erbium 3-μm fiber laser.

4 Conclusions

ESA spectra of ZBLAN:Er^{3+} were measured in the wavelength range 780–840 nm. The cross sections of ESA from the metastable levels ${}^4I_{13/2}$ and ${}^4I_{11/2}$ were derived. The values of the peak cross sections are $1.4 \times 10^{-21}\,\mathrm{cm}^2$ at 793 nm (from ${}^4I_{13/2}$), $2.3 \times 10^{-21}\,\mathrm{cm}^2$ at 808 nm (from ${}^4I_{11/2}$), and $0.9 \times 10^{-21}\,\mathrm{cm}^2$ at 831 nm (from ${}^4I_{11/2}$). The ESA cross sections at 793 nm of $1.4 \times 10^{-21}\,\mathrm{cm}^2$ from the ${}^4I_{13/2}$ level and less than $0.1 \times 10^{-21}\,\mathrm{cm}^2$ from the ${}^4I_{11/2}$ level are in reasonable agreement with former results ob-

tained from a rate-equation simulation of the erbium 3-μm laser. Experimental results for the 850-nm and 1.6-μm laser lines under simultaneous lasing at 3 μm are well understood with the information obtained from the ESA spectra.

ESA from either the $^4I_{11/2}$ or the $^4I_{13/2}$ level is present over the whole GSA range, with ESA cross sections being generally larger than that of GSA, i.e., ESA losses cannot be avoided when pumping in the investigated wavelength range. This result confirms that the detrimental influence of pump ESA when operating the erbium 3-μm fiber laser has to be minimized by avoiding a high excitation of the laser levels [8]. If the lifetime of the lower laser level is quenched by co-doping with another rare-earth ion and depletion via pump ESA loses its positive influence, a wavelength of 979 nm will be advantageous for pumping a double-clad fiber laser at 3 μm.

Acknowledgements. Hansjürg Weder from the Institute of Applied Physics, University of Bern, is thanked for technical assistance. This work was supported in part by the Swiss Priority Program "Optique".

References

1. L. Esterowitz, R. Allen: SPIE Infrared Fiber Opt. **1048**, 129 (1989)
2. S.L. Jacques, G. Gofstein: SPIE Laser-Tissue Interact. II **1427**, 63 (1991)
3. M. Ith, H. Pratisto, H.J. Altermatt, M. Frenz, H.P. Weber: Appl. Phys. B **59**, 621 (1994)
4. L. Esterowitz, R. Allen, I. Aggarwal: In Advanced Solid-State Lasers, 1991, Technical Digest Series (Optical Society of America, Washington, D.C. 1991) pp. 160–162
5. S. Bedö, M. Pollnau, W. Lüthy, H.P. Weber: Opt. Commun. **116**, 81 (1995)
6. M. Pollnau, Ch. Ghisler, G. Bunea, M. Bunea, W. Lüthy, H.P. Weber: Appl. Phys. Lett. **66**, 3564 (1995)
7. M. Pollnau, Ch. Ghisler, W. Lüthy, H.P. Weber, J. Schneider, U.B. Unrau: Opt. Lett. **22**, 612 (1997)
8. M. Pollnau: IEEE J. Quantum Electron. **33**, 1982 (1997)
9. S. Zemon, G. Lambert, W.J. Miniscalco, R.W. Davies, B.T. Hall, R.C. Folweiler, T. Wei, L.J. Andrews, M.P. Singh: SPIE Fiber Laser Sources and Amplifiers II **1373**, 21 (1990)
10. R.I. Laming, S.B. Poole, E.J. Tarbox: Opt. Lett. **13**, 1084 (1988)
11. M. Pollnau, E. Heumann, G. Huber: Appl. Phys. A **54**, 404 (1992)
12. J. Koetke, G. Huber: Appl. Phys. B **61**, 151 (1995)
13. M. Pollnau, W. Lüthy, H.P. Weber, K. Krämer, H.U. Güdel, R.A. McFarlane: Appl. Phys. B **62**, 339 (1996)
14. T. Danger, J. Koetke, R. Brede, E. Heumann, G. Huber, B.H.T. Chai: J. Appl. Phys. **76**, 1413 (1994)
15. L. Wetenkamp: Ph. D. dissertation, Institute of High-Frequency Technique, Technical University of Braunschweig, Germany 1991
16. R.S. Quimby, W.J. Miniscalco: Appl. Opt. **28**, 14 (1989)
17. M. Pollnau, R. Spring, Ch. Ghisler, S. Wittwer, W. Lüthy, H.P. Weber: IEEE J. Quantum Electron. **32**, 657 (1996)
18. J. Schneider, U.B. Unrau, M. Pollnau, W. Lüthy, H.P. Weber: "Depletion mechanisms of the 2.7-μm lower laser level $^4I_{13/2}$ in Er^{3+}-doped fibers", submitted
19. S.C. Goh: J. Non-Cryst. Solids **140**, 179 (1992)
20. R.S. Quimby, W.J. Miniscalco, B. Thompson: SPIE Fiber Laser Sources and Amplifiers III **1581**, 72 (1991)
21. R.C. Stoneman, J.G. Lynn, L. Esterowitz: IEEE J. Quantum Electron. **28**, 1041 (1992)